Appl Phys A (2010) 99: 39–46
DOI 10.1007/s00339-010-5576-5

Applied Physics A
Materials Science & Processing

Size parameter effect of dielectric small particle mediated nano-hole patterning on silicon wafer by femtosecond laser

Tetsuo Sakai · Yuto Tanaka · Yuji Nishizawa · Mitsuhiro Terakawa · Minoru Obara

Received: 10 November 2009 / Accepted: 22 January 2010 / Published online: 9 February 2010
© Springer-Verlag 2010

Abstract By use of a polystyrene particle with a fundamental (800 nm) and a second-harmonic (400 nm) wave of a femtosecond Ti:sapphire laser, nano-hole patterning properties on a silicon wafer were experimentally compared by keeping the size parameter constant. With the 800-nm wave, the patterned hole diameter ranged from 100 to 250 nm and the depth ranged from 20 to 100 nm. With the 400-nm wave, the hole diameter ranged from 50 to 200 nm while the depth ranged from 10 to 60 nm. The patterned diameter and the depth of patterned nano-holes were also controllable by the laser fluence. By the 3D finite-difference time-domain method it is numerically predicted that if the size parameter is kept at π approximately, the nano-hole patterning is efficiently performed even in the ultraviolet region of the spectrum.

1 Introduction

Fabrication of nano-periodic structures by using small particles is expected because it is a rapid process in atmospheric environment and a cost-effective, mask-less and dry process. In 2000, the Luk'yanchuk group demonstrated the nano-processing, which overcomes the diffraction limit by using a small particle, in laser cleaning experiments [1]. This processing mechanism stemmed mainly from the intense localized near-field light being generated around a small dielectric particle by laser irradiation. Using this scheme, an array of nano-dimple structures can be fabricated after ordering small particles periodically on a material surface [2–10]. Especially, nano-patterning of a silicon semiconductor surface is expected to be used for many applications such as an increase of data storage density [11, 12], efficiency improvement of solar cells [13] and control of the friction coefficient on a sliding surface for Micro Electro Mechanical Systems (MEMS) [14].

Femtosecond lasers have been used as a light source for generating near-field light, because it is appropriate for accurate micro-machining and can minimize a heat-affected zone [7, 8, 14–16]. Furthermore, femtosecond lasers can induce a multiphoton process due to their extremely high peak intensity, leading to the ablation processing of transparent materials at the laser wavelength [17–19]. Many articles concerning nano-processing of semiconductors using a femtosecond laser with dielectric small particles have dealt with the hole size, incident fluence effect [7–9, 14–16, 20], etc. The Bäuerle group reported briefly the laser-induced nano-patterning of silicon by three wavelengths of a femtosecond laser [8]. They used a regular lattice of amorphous silica micro-spheres as a micro-lens system for laser-induced single-step fabrication of arrays of nano-holes on a (100) Si surface. With single 265.7-nm femtosecond laser irradiation mediated with a 2D array of silica spheres of 300-nm diameter, hole diameters of 57 nm and depths of 6 nm were fabricated.

The size parameter ($\alpha = 2\pi r/\lambda$, r: radius of particle, λ: incident wavelength) in the Mie scattering theory is a critical parameter in the generation of near-field light by small dielectric spheres. The comprehensive relationship between the size parameter and the nano-hole size fabricated by femtosecond laser processing is not fully clarified yet.

In this paper, we report on the dependence of the size parameter in the Mie scattering theory on the nano-processing properties with small polystyrene (PS) particles. In the ex-

T. Sakai · Y. Tanaka · Y. Nishizawa · M. Terakawa · M. Obara (✉)
Department of Electronics and Electrical Engineering, Faculty of Science and Technology, Keio University, 3-14-1 Hiyoshi, Kohoku-ku, Yokohama 223-8522, Japan
e-mail: obara@obara.elec.keio.ac.jp

periment, we used two wavelengths (800 nm and 400 nm) of femtosecond laser pulses, which can demonstrate more precise processing than nanosecond laser pulses [15], and used a silicon wafer as used in advanced silicon electronic industries. A small PS particle was used as a dielectric particle, because it has a comparatively higher refractive index than the other dielectric particles and many PS particle sizes are commercially available. We theoretically focused on the near-field generation efficiency in three wavelengths using Mie theory and the experimental results were explained by the near-field distribution calculated with the 3D finite-difference time-domain (FDTD) method.

2 Experimental procedure

In the experiment, silicon ($10 \times 30 \times 0.5$ mm^3) wafers were used as substrate material. Silicon is an indirect transition semiconductor and therefore its multiphoton absorption coefficient becomes much larger than its linear absorption coefficient in the high-intensity region: for example at 800-nm laser intensities in excess of 10^{14} W/cm^2 its two-photon absorption is larger than its linear absorption. A polystyrene particle (Duke Scientific), which is transparent in the near-infrared ($\lambda = 800$ nm) and visible ($\lambda = 400$ nm) spectra, was selected as a dielectric small particle. The standard deviation of PS particle size is less than 3%. Table 1 lists the refractive index and extinction coefficient for PS and silicon used in this study [21]. Here, we used the refractive index of *small particle* PS at longer wavelengths than 280 nm [22] and we neglected the extinction coefficient k in this spectral region, because k is significantly small in this region. In the spectral domain ranging from 230 nm to 280 nm, we used the refractive index of *small particle* PS and the extinction coefficient of *bulk* PS [23, 24]. Below 230 nm, we used the refractive index and extinction coefficient of *bulk* PS. Monodispersed spherical PS particles with diameter of 800 nm or 450 nm were deposited and ordered in a hexagonal array on the silicon substrate by droplet suspension [25]. As shown in Fig. 1, the PS particles were well ordered on the silicon substrate. The experiments of near-field ablation processing were performed using a Ti:sapphire chirped pulse amplification (CPA) laser system. The laser pulses, with duration of 150 fs, center wavelength of 800 nm and energy of 1 mJ/pulse, were delivered at a repetition rate of 1 kHz. We also prepared a SHG (second harmonic generation) device (Cyber Laser Inc.) to generate a 400-nm SHG pulse. The pulse duration of the SHG is 350 fs approximately. The beams of both wavelengths had a Gaussian profile. We irradiated one pulse of a linearly polarized laser to the sample. The incident pulse at 800 nm and 400 nm was focused by a convex lens with focal length of 250 mm and 200 mm, respectively. The laser fluence of both 800 nm and 400 nm

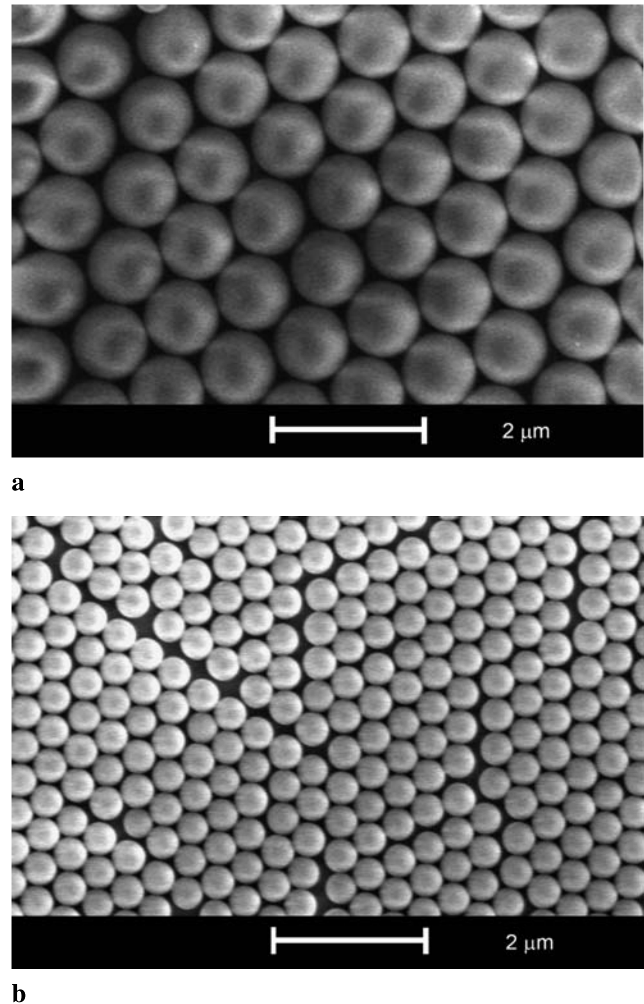

Fig. 1 SEM images of ordered monolayer PS particles in hexagonal array on silicon substrate. **a** The diameter is 800 nm. **b** The diameter is 450 nm

was varied from 0.1 to 1.0 J/cm^2 using an adjustable attenuator. The laser fluence was based on Refs. [26, 27]. Here, the laser fluence means the averaged laser fluence. The PS particles were removed after a single femtosecond laser pulse irradiation. To observe patterned surfaces no chemical cleaning treatments were conducted on the substrate surface after the laser ablation. The laser-induced nano-patterned Si surface was observed by scanning electron microscopy (SEM, Sirion, FEI Co.) and atomic force microscopy (AFM, SPI3800N, Seiko Instruments).

3 Localized near-field calculation using 3D FDTD

We used the 3D FDTD method to calculate the localized electric field distribution on and inside the Si substrate. This method, based on Maxwell's equations, is proven [28, 29] to give an accurate distribution of the electromagnetic field in the near and far field in the structures with arbitrary shapes.

Table 1 Refractive index and extinction coefficient for the materials used in the calculation

Wavelength [nm]		Dielectric function			
		Polystyrene		Silicon	
		n	k	n	k
200	*	2.3700	0.8770	–	–
263.5	**	1.7436	0.0103	1.764	4.278
400	***	1.6055	0.0000	5.570	0.387
800	***	1.5782	0.0000	3.673	0.005

*Both n and k are the values of bulk PS

**n is the value of small particle PS and k is the value of bulk PS

***Both n and k are the values of small particle PS

Two structure systems were mainly simulated: an isolated dielectric particle in vacuum environment and seven dielectric particles hexagonally ordered placed on a silicon substrate. The electric field strength of the incident light is assumed as 1 V/m. We used the optical properties of the investigated materials listed in Table 1.

4 Near-field efficiency calculated by Mie scattering theory

A near field generated in the vicinity of a dielectric particle induces a nano-scale hole on the Si surface whose diameter is much smaller than the incident wavelength. The near-field efficiency that is of importance for the laser nano-processing can be derived from the Mie scattering theory [30]. Here, we consider an isolated small particle system, whose near-field efficiency is obtained by integrating the scattering electric field around the particle. In 1981 Messinger et al. introduced the following equation to calculate the near-field efficiency [31]:

$$Q_{\mathrm{nf}}(R) = 2\frac{R^2}{r^2}\sum_{n=1}^{\infty}\Big\{|a_n|^2\Big[(n+1)\big|h_{n-1}^{(1)}(\kappa R)\big|^2 + n\big|h_{n+1}^{(1)}(\kappa R)\big|^2\Big] + (2n+1)|b_n|^2\big|h_n^{(1)}(\kappa R)\big|^2\Big\}, \tag{1}$$

where r is the radius of the small particle, R is the distance from the center of the small particle, a_n and b_n are Mie scattering coefficients and $h_n^{(1)}$ is a spherical Hankel function. κ is the wave number defined with the refractive index of the surrounding medium n_M outside the particle ($\kappa = 2\pi n_M/\lambda$).

Figure 2 shows the dependence of the near-field efficiency Q_{nf} on the size parameter for four wavelengths. The near-field efficiency Q_{nf} was calculated at the position of the particle surface $R = r$. Shown in Fig. 2 are the near-field efficiencies for the four wavelengths, which are 800 nm (fun-

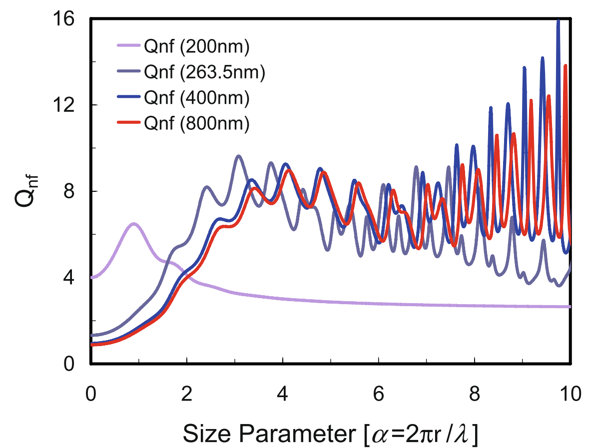

Fig. 2 Dependence of the near-field efficiency on the size parameter for four wavelengths. The near-field efficiency Q_{nf} is calculated at $R = r$ and starting from $\alpha = 0.01$

damental wave), 400 nm (SHG), 263.5 nm (THG: third harmonic generation of 800 nm), and 200 nm. The near-field efficiencies at 800 nm and 400 nm seem to be similar, as can be seen in Fig. 2. This result means that the similar near-field efficiency can be excited at both wavelengths, if the ratio of the incident wavelength to the particle size is kept constant. When the incident wavelength is shortened to 263.5 nm, a different tendency from those of 800 nm and 400 nm is shown. The near-field efficiency decreases with the increase of the size parameter due to the absorption of the PS particle itself, which can be understood by the increase in the extinction coefficient k at shorter wavelengths. A strong absorption appears around 260 nm, according to the PS absorption spectra [32] (see Table 1). In the case of the incident wavelength of 200 nm, the near-field efficiency shows a quite different behavior. The near-field efficiency reaches a maximum value in the range of small size parameter and it rapidly decreases with increasing size parameter. From the calculated result and the extinction coefficient, it was found that PS behaves similarly to small metal particles, that is, the near-field efficiency shows a similar tendency. However, because the near-field efficiency of PS particles is not as high as that of metal particles [33, 34], it is difficult to induce a nano-hole patterning using a PS particle and shorter wavelengths below 260 nm.

Figure 3 shows the dependence of the near-field efficiency on the incident wavelength for four size parameters. According to this, the diameter of the nano-hole patterning is decreased with the decrease of the size parameter [7], and we selected the four size parameters. As previously described in Sect. 2, we used the refractive index of bulk PS for incident wavelengths ranging from 280 nm to 200 nm, resulting in a precipitous change on each curve at 280 nm. Red, blue and blue gray dashed lines show the change in the near-field efficiency at the incident wavelengths of 800, 400 and 263.5 nm, respectively. The near-field efficiency for

each size parameter changes slowly down to 300 nm, and an abrupt change is observed below 300 nm. Since the PS particle itself has a large absorption coefficient at 200 nm, the near-field efficiency decreases significantly. Hence, incident wavelengths useful for the PS-mediated nano-processing are found to be longer than 260 nm.

5 Electric field intensity distribution near the PS particle calculated by 3D FDTD method

From the results shown in Fig. 3, it is concluded that the applicable incident wavelength for near-field nano-processing using a PS particle is longer than 260 nm for every size parameter.

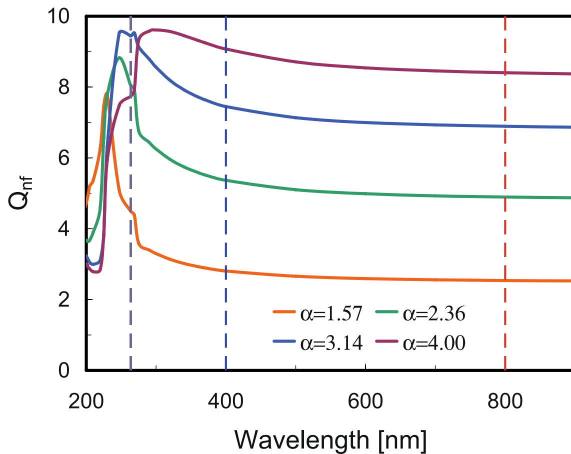

Fig. 3 Dependence of the near-field efficiency on the incident wavelength for four size parameters. The near-field efficiency Q_{nf} is calculated at $R = r$. *Deep blue*, *blue* and *red dashed lines* show the wavelengths of 263.5, 400 and 800 nm, respectively

Figure 4 shows the electric field intensity distribution for two size parameters, using three incident wavelengths. The calculation was performed for the system where a single PS particle is placed isolated in vacuum. Figure 4a, b and c show the electric field distribution when the size parameter is $\alpha \sim 3.14$ at 800, 400 and 263.5 nm, respectively ($\alpha = 3.10$ only at 263.5 nm). The white dashed line delineates the PS particle in the simulation. The incident polarization is parallel to the x axis, and the incident plane wave is directed along the $-z$ direction. For the size parameter $\alpha \sim 3.14$, the incident wavelength is equivalent to the diameter of the PS particle. The forward scattering distribution predicted uniquely by the Mie scattering can be confirmed for all electric field distributions. Furthermore, a strongly focused electric field intensity spot is observed inside the PS particle, indicating that the PS particle acts as a micro-lens. This electric field inside the particle induces the near field under the particle, because it is focused at the bottom section of the particle to induce a strong electric field intensity. Figure 4d, e and f show the electric field distribution when the size parameter is $\alpha \sim 1.57$ for 800, 400 and 263.5 nm, respectively ($\alpha = 1.55$ only at 263.5 nm). For the size parameter $\alpha \sim 1.57$, the diameter of the PS particle is about half the incident wavelength. The forward scattering distribution explained by the Mie scattering can also be confirmed for all of these electric field distributions. However, for this size parameter, the micro-lens effect disappears and the internal electric field intensity is much smaller than that of the size parameter of $\alpha \sim 3.14$. The near-field intensity of the scattering field induced by a PS particle smaller than the incident wavelength becomes smaller. Hence, the use of the smaller particle does not result in the uniform nano-processing [35].

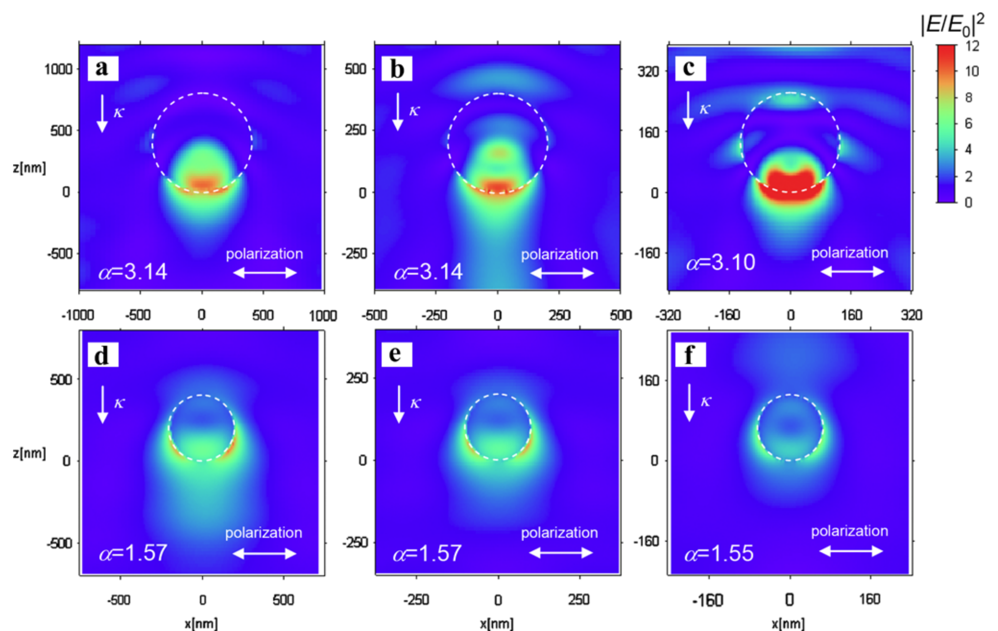

Fig. 4 Electric field intensity distribution (x–z plane, $y = 0$ nm) calculated by 3D FDTD method. The simulation is performed using PS particles with diameters of 800, 400 and 260 nm placed in vacuum. The incident wavelengths are 800, 400 and 263.5 nm directed along the $-z$ direction. The polarization is parallel to the x axis. White dashed lines delineate the PS particles. **a** Incident wavelength λ is 800 nm, PS diameter d is 800 nm. **b** $\lambda = 400$ nm, $d = 400$ nm. **c** $\lambda = 263.5$ nm, $d = 260$ nm. **d** $\lambda = 800$ nm, $d = 400$ nm. **e** $\lambda = 400$ nm, $d = 200$ nm. **f** $\lambda = 263.5$ nm, $d = 130$ nm

Even if the particle size and incident wavelength are decreased, the relationship between the size parameter and near-field efficiency does not show an appreciable change, and the calculated electric field intensity distributions are similar. Especially, in the system where the micro-lens effect is dominant, efficient nano-processing control by the near field is possible. In short, it is numerically predicted that if the size parameter is kept at π approximately, the nano-hole patterning is efficiently performed even in the ultraviolet (UV) region of the spectrum. We will discuss the electric field intensity distribution inside the silicon substrate at the size parameter $\alpha \sim 3.14$ in Sect. 6.

6 Electric field intensity distribution inside silicon wafer

We predicted that the size parameter suitable for efficient nano-processing is around $\alpha \sim 3.14$. Figure 5 shows the cross-sectional image of the electric field intensity distribution inside the silicon substrate for the size parameter $\alpha \sim 3.14$. White dashed lines delineate the surface of the PS particle, and the contour lines show the electric field intensity distribution inside the silicon substrate. As shown in Fig. 5a, the irradiated electric field is focused deeply inside the silicon substrate. Therefore, the incident electric field intensity is sufficiently enhanced by the micro-lens effect. Figure 5b shows the electric field intensity distribution inside the silicon substrate with 400-nm irradiation. Since the extinction coefficient k increases, the electric field intensity decreases drastically. Figure 5c shows the electric field intensity distribution inside the silicon substrate with 263.5-nm irradiation. In Sect. 5, we found that the highest near-field efficiency is induced in the vicinity of 263.5 nm. Furthermore, the electric field intensity generated at 263.5 nm for $\alpha \sim 3.14$ is larger than the ones at the other wavelengths (Fig. 4a–c). However, as can be seen in Fig. 5c, little penetration of the electric field into the Si substrate is observed and the field is mostly reflected off the substrate surface. It is because the extinction coefficient k of the silicon substrate at 263.5 nm has a similar value to metals (see Table 1). The use of 263.5-nm wavelength can provide a smaller hole processing and the patterned hole depth becomes shallow. Here, we are going to experimentally compare the nano-hole processing properties with 800 nm and 400 nm of the femtosecond laser pulse.

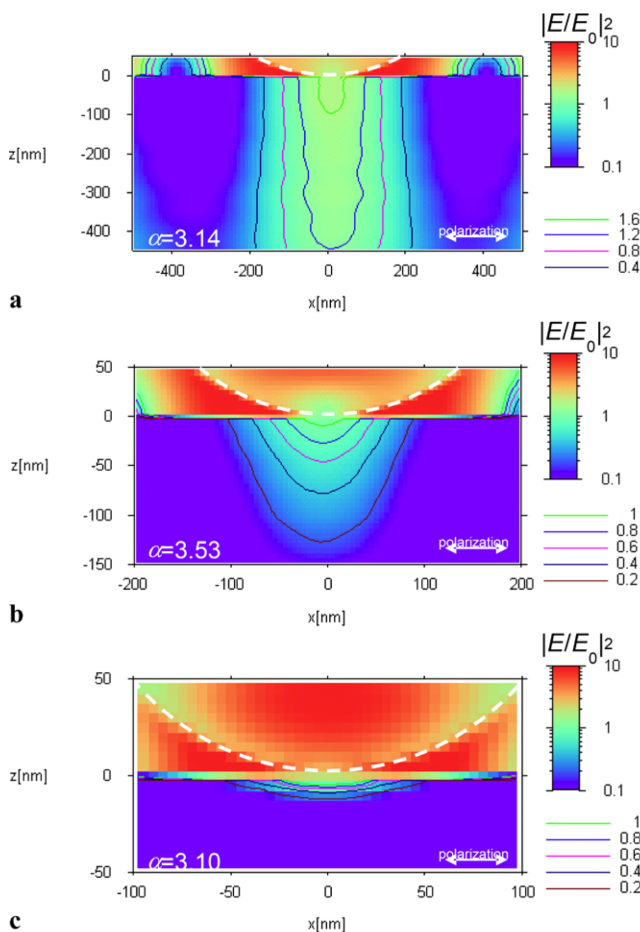

Fig. 5 Electric field intensity distribution in x–z plane under PS particle and inside silicon substrate. *White dashed line* shows the PS particle surface. The Si surface is at $z = 0$ nm. **a** Incident wavelength λ is 800 nm, the PS diameter d is 800 nm. **b** $\lambda = 400$ nm, $d = 450$ nm. We selected the diameter of 450 nm for the calculation, because this diameter was used experimentally. **c** $\lambda = 263.5$ nm, $d = 260$ nm

7 Nano-hole processing properties with 800-nm and 400-nm femtosecond laser pulse

7.1 Nano-hole processing results

Figure 6a and b show the SEM images of the Si substrate surface after irradiating a femtosecond laser pulse of 800 nm and 400 nm to the structure shown in Fig. 1a and b, respectively. The laser fluence is 288 $\mathrm{mJ/cm^2}$ at 800 nm and 57 $\mathrm{mJ/cm^2}$ at 400 nm. The ablation threshold fluence for a *bare* silicon substrate without PS particles was 252 $\mathrm{mJ/cm^2}$ at 800 nm and 57.8 $\mathrm{mJ/cm^2}$ at 400 nm. Both pictures show elongated shapes. These experimental results are in excellent agreement with the 3D FDTD results at an x–y plane, $z = -2.5$ nm in the silicon substrate, which are shown in Fig. 7a and b. The system of seven hexagonally ordered dielectric particles placed on a silicon substrate is simulated because the particles couple with each other. The experimentally fabricated nano-hole pattern is well explained by the calculated elliptical shape with the long axis perpendicular to the polarization of the incident light [35]. The circular polarization pulse gave a circular hole patterning [19].

Figure 8a and b show the AFM images of the patterned Si surface after irradiating a single laser pulse with linear polarization at 800 and 400 nm to the structure shown

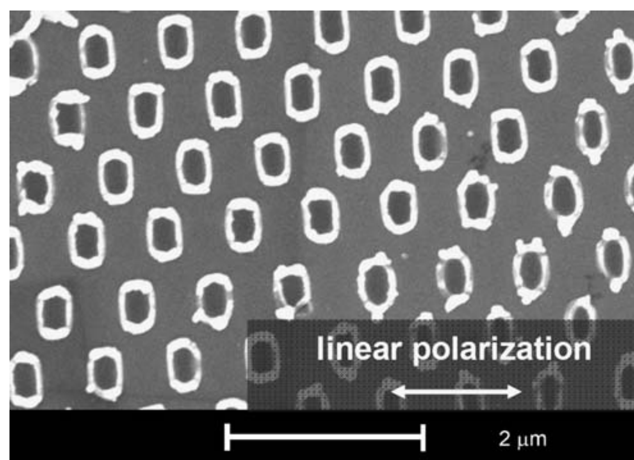

a

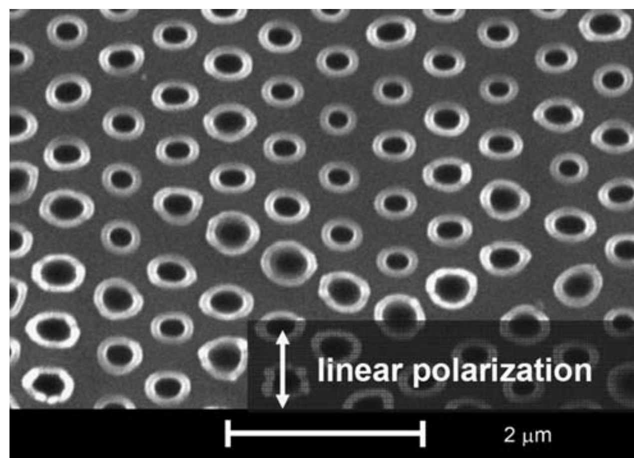

b

Fig. 6 SEM images of the Si surface after femtosecond laser irradiation. **a** 800 nm with fluence of 288 mJ/cm^2, **b** 400 nm with fluence of 57 mJ/cm^2

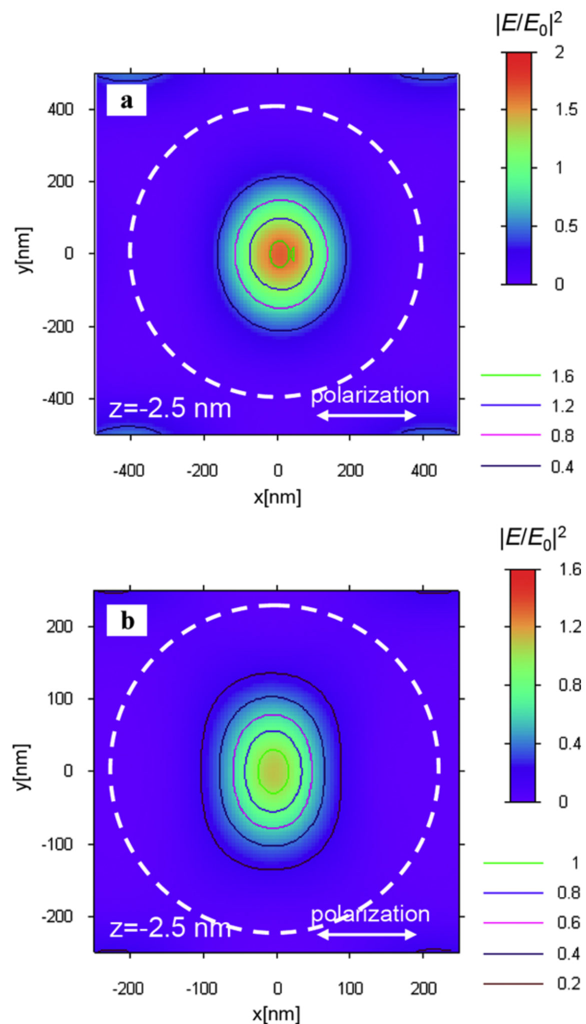

Fig. 7 Electric field intensity distribution calculated by 3D FDTD method (x–y plane, $z = -2.5$ nm). *White dashed line* shows the delineation of the PS particle. **a** Incident wavelength λ is 800 nm, PS diameter d is 800 nm ($\alpha = 3.14$). **b** Incident wavelength λ is 400 nm, PS diameter d is 450 nm ($\alpha = 3.53$)

in Fig. 1a and b, respectively. The fluence is 570 mJ/cm^2 at 800 nm and 290 mJ/cm^2 at 400 nm. To observe patterned surfaces no chemical etching treatments were conducted on the patterned silicon surface after laser irradiation. The Bäuerle group reported that just after laser patterning the nano-holes are surrounded by a ring-shaped rim [8]. This rim has been etched by dipping the sample in a 20% HF solution for about 2 min before AFM observation [8]. The depth of the nano-hole is observed to be quite shallow in both systems, as predicted by the 3D FDTD simulation as shown in Fig. 5. With the decrease of the incident laser wavelength, the extinction coefficient of silicon reduces the incident energy transfer into the Si substrate. Consequently, the fabricated hole depth becomes shallower.

The laser-induced nano-patterning of silicon by three wavelengths of a femtosecond laser was previously reported by the Bäuerle group [8]. They used a regular lattice of amorphous silica micro-spheres for laser-induced single-step fabrication of arrays of nano-holes on a Si surface. With a single 265.7-nm femtosecond laser irradiation mediated with a 2D array of silica spheres of 300-nm diameter, hole diameters of 57 nm and depths of 6 nm were fabricated. This experimental result is well explained by our simulation result.

7.2 Effect of laser fluence

Changing particle size can control the diameter and depth of the patterned nano-holes. Figure 9 shows the dependence of the diameter and depth of patterned nano-holes on the laser fluence for the two wavelengths. Red and blue dashed lines in Fig. 9 indicate the ablation threshold of the bulk silicon without PS particle mediation. The diameter and the depth are increased linearly with the increase

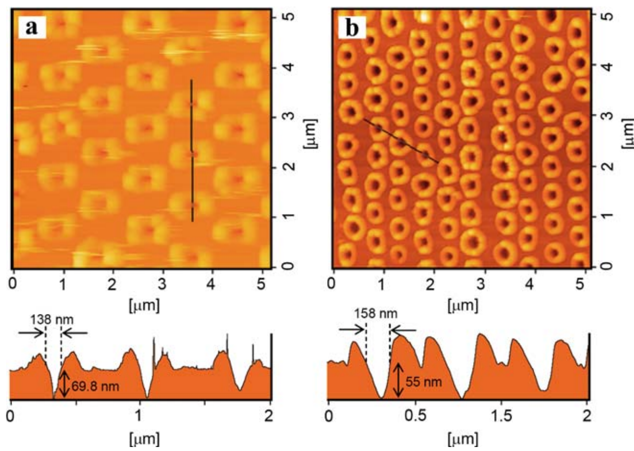

Fig. 8 AFM images of the Si surface after laser irradiation. Cross-sectional images in the bottom figures correspond to the positions of the *black lines* in the *top figures*. **a** 800-nm laser with fluence of 570 mJ/cm^2 was irradiated to the structure shown in Fig. 1a. **b** 400-nm laser with fluence of 290 mJ/cm^2 was irradiated to the structure shown in Fig. 1b

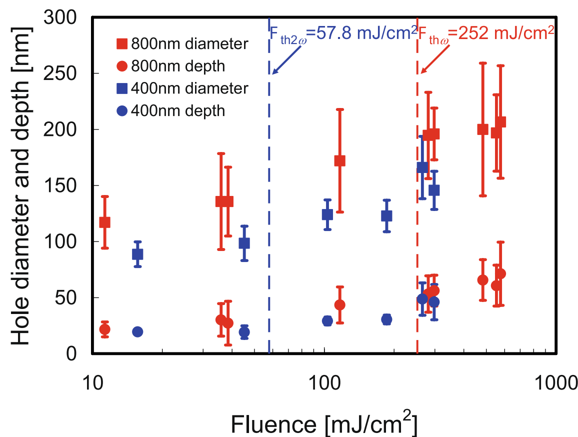

Fig. 9 Plots of diameter and depth of nano-holes as a function of laser fluence. *Red dashed line* represents the ablation threshold fluence for bare silicon with 800-nm femtosecond laser pulse. *Blue dashed line* represents the ablation threshold fluence for bare silicon with 400-nm femtosecond laser pulse. *Red* and *blue plots* show the diameter and the depth of nano-holes fabricated with 800-nm and 400-nm irradiation, respectively. *Square plots* show the length of the short axis of the nano-holes. *Circular plots* show the depth of the nano-holes

of the fluence. This experimental result seems to be similar to that with small gold particles [36]. The maximum nano-hole depth fabricated by the 800-nm laser is about 100 nm, which is two times deeper than that at 400-nm wavelength. According to the calculation results in Fig. 5a and b, the nano-hole depth is dependent upon the energy transfer efficiency into the silicon substrate, which is evidenced by the experiment. With the 800-nm laser, the patterned hole diameter experimentally ranged from 100 to 250 nm and the depth ranged from 20 to 100 nm. With the 400-nm SHG wave, the patterned hole diameter ranged from 50 to 200 nm and the depth ranged from 10 to 60 nm.

8 Conclusion

Nano-processing properties of a silicon surface were presented from the viewpoint of the size parameter in the Mie scattering theory. By use of PS particles with fundamental (800 nm) and SHG (400 nm) waves of a femtosecond Ti:sapphire laser, nano-processing properties were experimentally compared by keeping the size parameter constant. The near-field distribution and enhanced localized field were numerically simulated as a function of the size parameter using the 3D FDTD method. It is numerically predicted that if the size parameter is kept at π approximately, the nano-hole patterning is efficiently performed even in the ultraviolet (UV) region of the spectrum. In the UV spectral region, wide-band-gap particles are, of course, necessary. The patterned diameter and the depth of the nano-holes were also controllable by the laser fluence. With the 800-nm laser with 150-fs duration, the patterned hole diameter experimentally ranged from 100 to 250 nm and the depth ranged from 20 to 100 nm. With the 400-nm SHG wave with 350-fs duration, the hole diameter ranged from 50 to 200 nm and the depth ranged from 10 to 60 nm. With the decrease of the incident laser wavelength, the extinction coefficient of silicon reduced the incident energy transfer into the Si substrate, so that the fabricated hole depth becomes shallower.

Acknowledgements This work is supported in part by a Grant-in-Aid for the Global Center of Excellence for High-Level Global Cooperation for Leading-Edge Platform on Access Spaces from the Ministry of Education, Culture, Sport, Science and Technology, Japan. T. Sakai is grateful for a JSPS Fellowship for Young Scientists.

References

1. Y.F. Lu, L. Zhang, W.D. Song, Y.W. Zheng, B.S. Luk'yanchuk, JETP Lett. **72**, 457 (2000)
2. O. Watanabe, T. Ikawa, M. Hasegawa, M. Tsuchimori, Y. Kawata, Appl. Phys. Lett. **79**, 1366 (2001)
3. T. Ikawa, T. Mitsuoka, M. Hasegawa, M. Tsuchimori, O. Watanabe, Y. Kawata, Phys. Rev. B **64**, 195408 (2001)
4. S. Theppakuttai, S. Chen, Appl. Phys. Lett. **83**, 758 (2003)
5. Z.B. Wang, M.H. Hong, B.S. Luk'yanchuk, S.M. Huang, Q.F. Wang, L.P. Shi, T.C. Chong, Appl. Phys. A **79**, 1603 (2004)
6. Z.B. Wang, M.H. Hong, B.S. Luk'yanchuk, Y. Lin, Q.F. Wang, T.C. Chong, J. Appl. Phys. **96**, 6845 (2004)
7. H. Takada, M. Obara, Jpn. J. Appl. Phys. **44**, 7993 (2005)
8. D. Brodoceanu, L. Landstorm, D. Bäuerle, Appl. Phys. A **86**, 313 (2007)
9. W. Guo, Z.B. Wang, L. Li, Z. Liu, B. Luk'yanchuk, D.J. Whitehead, Nanotechnology **19**, 455302 (2008)
10. S.M. Huang, Z.A. Wang, Z. Sun, Z.B. Wang, B.S. Luk'yanchuk, Appl. Phys. A **96**, 459 (2009)
11. P.R. Krauss, S.Y. Chou, Appl. Phys. Lett. **71**, 3174 (1997)

12. M.H. Hong, F. Ma, C.S. Lim, Y. Lin, Z.Q. Huang, L.S. Tan, L.P. Shi, T.C. Chong, in *APLS 2008 Int. Conf.*, Nagoya, Japan, 30 January–1 February 2008
13. H.L. Chen, S.Y. Chuang, C.H. Lin, Y.H. Lin, Opt. Express **15**, 14793 (2007)
14. T. Sakai, N. Nedyalkov, M. Obara, J. Phys. D, Appl. Phys. **40**, 7485 (2007)
15. H.-J. Münzer, M. Mosbacher, M. Bertsch, J. Zimmermann, P. Leiderer, J. Boneberg, J. Microsc. **202**, 129 (2001)
16. M. Mosbacher, H.-J. Münzer, J. Zimmermann, J. Solis, J. Boneberg, P. Leiderer, Appl. Phys. A **72**, 41 (2001)
17. Y. Zhou, M.H. Hong, J.Y.H. Fuh, L. Lu, B.S. Luk'yanchuk, Z.B. Wang, L.P. Shi, T.C. Chong, Appl. Phys. Lett. **88**, 023110 (2006)
18. Y. Zhou, M.H. Hong, J.Y.H. Fuh, L. Lu, B.S. Luk'yanchuk, Z.B. Wang, J. Alloys Compd. **449**, 246 (2008)
19. T. Sakai, N. Nedyalkov, M. Obara, J. Phys. D, Appl. Phys. **40**, 2102 (2007)
20. J. Boneberg, J. Konig-birk, H.-J. Munzer, P. Leiderer, K.L. Shuford, G.C. Schatz, Appl. Phys. A **89**, 299 (2007)
21. D.R. Lide (ed.), *CRC Handbook of Chemistry and Physics*, 84th edn. (CRC Press, Boca Raton, 2004)
22. X. Ma, J.Q. Lu, R.S. Brock, K.M. Jacobs, P. Yang, X.-H. Hu, Phys. Med. Biol. **48**, 4165 (2003)
23. T. Inagaki, E.T. Arakawa, R.N. Hamm, M.W. Williams, Phys. Rev. B **15**, 3243 (1977)
24. W.L. Buck, B.R. Thomas, A. Weinreb, J. Chem. Phys. **48**, 549 (1968)
25. E. Adachi, A.S. Dimitrov, K. Nagayama, Langmuir **11**, 1057 (1995)
26. S. Baudach, J. Bonse, W. Kautek, Appl. Phys. A **69**, S395 (1999)
27. J. Bonse, P. Rudolph, J. Krüger, S. Baudach, W. Kautek, Appl. Surf. Sci. **154**, 659 (2000)
28. A. Taflove, S.C. Hagness, *Computational Electrodynamics: The Finite-Difference Time-Domain Method* (Artech House, Boston, 2000)
29. K. Sendur, W. Challener, C. Peng, J. Appl. Phys. **96**, 2743 (2004)
30. G. Mie, Ann. Phys. (Leipz.) **25**, 377 (1908)
31. B.J. Messinger, K.U. von Raben, R.K. Chang, P.W. Barber, Phys. Rev. B **24**, 649 (1981)
32. R.H. Boundy, R.F. Boyer, *Styrene, its Polymers, Copolymers, and Derivatives* (Reinhold, New York, 1952)
33. N. Nedyalkov, H. Takada, M. Obara, Appl. Phys. A **85**, 163 (2006)
34. N. Nedyalkov, T. Sakai, T. Miyanishi, M. Obara, J. Phys. D, Appl. Phys. **39**, 5037 (2006)
35. T. Sakai, T. Miyanishi, N. Nedyalkov, Y. Nishizawa, M. Obara, J. Phys. D, Appl. Phys. **42**, 025502 (2009)
36. D. Eversole, B. Luk'yanchuk, A. Ben-Yakar, Appl. Phys. A **89**, 283 (2007)